Control of Spatial Deposition of Electrospun Fiber Using Electric Field Manipulation

Abdul Hamid Nurfaizey[1,2,3], Jonathan Stanger[1,3,4], Nick Tucker[3], Neil Buunk[4], Alan R. Wood[5], Mark P. Staiger[1]

[1]Department of Mechanical Engineering, University of Canterbury, NEW ZEALAND

[2]Faculty of Mechanical Engineering, Universiti Teknikal Malaysia Melaka, MALAYSIA

[3]The New Zealand Institute for Plant & Food Research Limited, NEW ZEALAND

[4]Electrospinz Ltd, Blenheim, NEW ZEALAND

[5]Department of Electrical and Computer Engineering, University of Canterbury, NEW ZEALAND

Correspondence to:
Nick Tucker email: Nick.Tucker@plantandfood.co.nz

ABSTRACT

A significant challenge in the synthesis of uniform membranes via electrospinning is achieving a spatially uniform deposition of electrospun fibers. The problem is more pronounced in the case of a multi-spinneret system due to self repulsion between the jets. In this study, electric field manipulation (*via* auxiliary electrodes) is explored as a potential technique for controlling the spatial deposition area of electrospun fiber. It was observed experimentally that the location and size of the deposition area can be moved linearly in response to the applied voltages at the auxiliary electrodes. Finite element analysis (FEA) was used to simulate the electric field strength and distribution at a given applied voltage and its effect on the flight path of electrospun fiber. Comparisons between experiments and simulations were made in evaluating the accuracy of simulations. The adaptation of this technique in production would provide a method of controlled deposition for producing uniform electrospun fiber membranes.

INTRODUCTION

Electrospinning is a processing method for the synthesis of continuous polymeric fibers with cross-sectional dimensions in the submicron range. Although the method has long been introduced, it regained interest recently when it was reintroduced by Doshi *et al.* [1]. A historical review of electrospinning was recently provided by Tucker *et al.* [2]. Electrospinning was first described in patents by Cooley [3] and Morton [4]. Between 1934 and 1944 a sequence of patents were then granted to Formhals on the method and apparatus of producing "artificial threads" [5].

Electrospinning begins with a droplet of polymer (either in solution or molten phase) subjected to a high voltage at some distance from a grounded or oppositely charged collector. Typically, the charged polymer solution or melt is delivered through a narrow spinneret (sometimes described as a needle or nozzle). Under the influence of a high strength electric field, the shape of the droplet is distorted until at a critical field gradient, the electric forces applied overcome the surface tension of the droplet, and a stream or jet is ejected from the droplet. The distorted droplet forms a conical shape known as the Taylor cone as the electrospinning process attains equilibrium [6].

Initially, the solution jet travels in a straight line for a distance until a bending (or whipping) instability occurs whereupon the flight path diverges into an expanding helix. The diameter of the jet is decreased due to stretching caused by the whipping instability, leading to the submicron diameters typically observed. The deposition of solid phase fibers at the collector from a polymer solution or melt occurs due to rapid solvent loss or cooling, respectively. Typically, electrospinning results in a thin mat of fibers exhibiting a randomly arranged architecture.

One of the issues limiting the application of electrospun fibers at an industrial scale is the low output of the process [7]. A multi-spinneret system is often used to increase productivity. However, a multi-spinneret system can result in variations in the density of deposition within an electrospun mat as the result of electrostatic repulsion between adjacent jets

[8]. The pattern that develops as a consequence of the variation in fiber density appears as a series of alternating darker and lighter stripes on the collector.

Various multi-spinneret setups with laterally moving collectors or spinning heads have been described with the aim of producing uniform coverage of electrospun fibers [9]. However, setups based on these techniques are mechanically complex due to the moving components. Another alternative is electrospinning from a free liquid surface without using spinnerets [10]. Although electrospinning without a spinneret is mechanically simple, the process itself is complex due to the random formation of the jets and it is often associated with thicker fiber diameters [11].

Non-mechanical approaches to deposition control based on electric field manipulation are reported. The method exploits repulsive columbic forces to influence the flight path of the electrospun fibers. For example, Deitzel *et al.* [12] used eight ring auxiliary electrodes to eliminate the whipping instability, thereby reducing the deposition area. Bellan *et al.* [13] showed that the speed of such methods was sufficient to align a single fiber by cyclically varying the applied voltage *via* a split ring auxiliary electrode. Electric field manipulation *via* a cylindrical auxiliary electrode was applied to multi-spinneret to reduce the size of the deposition area [14]. The present authors also reported on the superposition principle of electric fields as a method of controlled deposition in electrospinning [15].

The effects of changing the set-up geometry and process parameters on electrospinning have been described using Finite Element Analysis (FEA). Heikkila et al. [16] used FEA to determine the 3D electric field as a function of spinning distance and voltage, and the effect on the size, shape and diameter of the fibers. Cui et al. [17] used FEA to visualise the electric field distribution of a modified electrospinning setup that consisted of a spinneret protruding through a metal plate and a series of focusing rings. Angammana and Jayaram [18] used FEA to show that scaling up from a single to dual spinneret arrangement reduces the local electric field at the spinneret, necessitating a higher applied voltage to initiate electrospinning.

In this study, the objectives are to (i) demonstrate the use of electric field manipulation to control the direction and size of the deposition area and (ii) explore the relevance of FEA for prediction of the flight path of electrospun fiber. The spatial shift and size of the deposition area as a function of voltage difference between two auxiliary electrodes is measured quantitatively, while the FEA model is designed to emulate the experimental observations by simulating the change of magnitude and direction of the electric field. In this work, the emphasis is on the control of the spatial location and size of a random deposited fiber mat rather than aligned deposition of a single fiber.

EXPERIMENTAL PROCEDURES

Materials

An aqueous solution of poly(vinyl alcohol) (PVOH) (Chemiplas NZ limited, New Zealand) with a final PVOH concentration of 8 wt.% was used for electrospinning. The PVOH had an average molecular weight of 118,000 $gmol^{-1}$ and degree of hydrolysis (DH) in the range of 85–90%. The polymer solution was prepared by dissolving PVOH in distilled water for approximately 2 h at 60°C.

Electrospinning apparatus

Electrospinning was carried out using a modified commercial laboratory scale machine (Model ES4, Electrospinz Ltd., New Zealand). A constant potential difference of +10 kV and distance of 100 mm was used between the spinneret and a grounded collector (*Figure 1*). Two independent auxiliary electrodes were fixed in position either side of the spinneret, with the voltage difference varied between 0 and +12 kV, and their voltage controlled independently of the spinneret voltage.

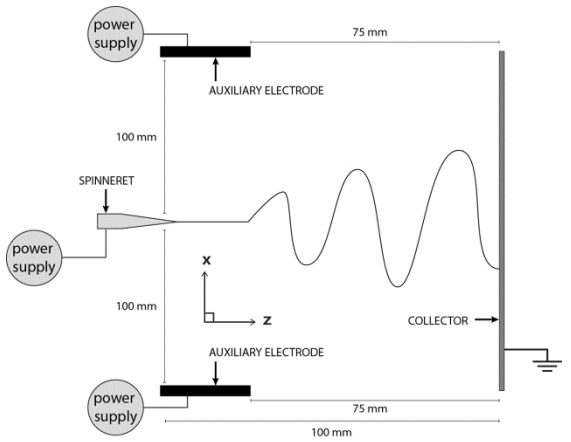

FIGURE 1. Plan view of the electrode arrangement used to control the spatial location and size of the deposition area.

Two different types of experiments were conducted for which (i) a single auxiliary electrode was charged while the other was held at zero voltage (E1); and (ii) both auxiliary electrodes were charged with voltage combinations between +2 to +10 kV (E2) (*Table I*). A reversed order of voltage combination was also

used for E1 and E2 to demonstrate that the arrangement was acceptably symmetrical. E1 was conducted to ascertain the maximum possible shift in the deposition area (L_{exp}) that could be obtained using the described apparatus and parameters. Meanwhile E2 was conducted to determine if the base voltage (V_b) (*i.e.* lower of the two auxiliary electrode voltages) influences the shift in the deposition area.

A naming convention is adopted here to describe the applied voltages and the manner in which they were applied. For example, 8-2 kV indicates a voltage of 8 kV and 2 kV was applied to the left and right electrodes (*Figure 1*), respectively, giving a voltage difference (V_d) of +6 kV and base voltage (V_b) of +2 kV. Changes in shift of the deposition area were measured relative to a default condition (*Table I*). Samples of the electrospun mat were produced in triplicate.

TABLE I. The various voltage combinations used to charge the auxiliary electrodes in E1 and E2. *N.B.* * indicates the default condition used for comparisons.

	Applied voltages (kV)	**Total samples**
E1	0-0* 2-0, 4-0, 6-0, 8-0, 10-0, 12-0 0-2, 0-4, 0-6, 0-8, 0-10, 0-12	39
E2	2-2*, 4-4*, 6-6*, 8-8* 2-4, 2-6, 2-8, 4-6, 4-8, 4-10, 6-8, 6-10, 8-10 4-2, 6-2, 8-2, 6-4, 8-4, 10-4, 8-6, 10-6, 10-8	66

A 300 × 300 mm sheet of 316 stainless steel was attached to the high density polyethylene backplane of the ES4 apparatus to be used as the grounded collector electrode. A sheet of A4 80 g/m^2 Kaskad Raven Black paper (no. 1516RB) was mounted in a registered position onto the collector to aid visualisation of the deposited fiber. The as-deposited electrospun mats were then scanned at a resolution of 300 dpi and converted to 2481 × 3509 pixel JPEG images.

Image analysis (UTHSCSA ImageTool, Version 3.0) was used to measure the x-y coordinates of the centre to give the magnitude of shift of the deposited mat (L_{exp}). Similarly, the average size of the deposition area in x and y axes was measured using image analysis to get the aspect ratio. The aspect ratio is defined as the ratio of the width of deposition area to its height. Three measurements were taken during image analysis to get an average. Linear regression was used to model the relationship between V_d, V_b, L_{exp} and aspect ratio. Scatter plots of L_{exp} as a function of V_d; and aspect ratio as a function of V_b were made and best fit lines were fitted to the plots.

Scanning Electron Microscopy

SEM microscopy images were taken using JEOL Neoscope (JCM-5000). The as-spun fibers on black paper were cut into 1 × 1 cm^2 and mounted onto an aluminum stub. The samples were then sputtered with gold for 120 seconds (Quorum Q150R). From the SEM images, the average fiber diameters were measured using Electrospinz SEM Analyzer software (Electrospinz Ltd., New Zealand).

Finite Element Analysis

The COMSOL microelectromechanical systems (MEMS) module (Version 3.5a) was used to model the experimental setup, with electric voltage as the dependent variable. The 3D model of the electrospinning apparatus in *Figure 1* was drawn within a cubic boundary measuring 2 × 2 × 2 m. The alignment of the auxiliary electrodes and spinneret were made parallel with the x axis, while the deposition direction of fiber is parallel with the z axis. The model calculations were restricted to the region of interest between the spinneret, auxiliary electrodes and collector. The spinneret was charged at +10 kV whilst the collector and outer boundary were grounded. The voltage at the auxiliary electrodes was varied to replicate the experimental values used in *Table I*.

To quantify the effect of V_d on the direction of electrospun fiber in flight, the magnitude and direction of electric field component E_x along the z axis (*Figure 2*) between the spinneret and collector was plotted. Separately, two electric field plots of E_x and E_y were also made to replicate the effect when both electrodes were charged at a given voltage. The plots were made to represent the electric field along two intersecting axes (200 mm in length) labelled as x'-x" and y'-y" which were drawn on an imaginary plane mid-way between the spinneret and collector (*Figure 2*).

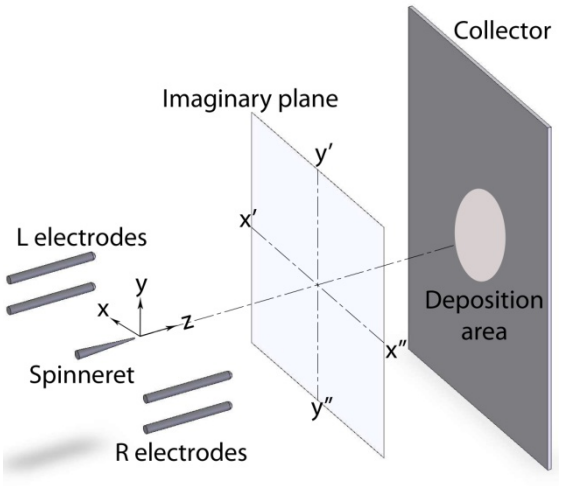

FIGURE 2. A schematic illustrating the arbitrarily-selected z axis and imaginary plane used for quantifying the electric field strength.

In post-processing mode, particle tracing option was used to trace the path of a charged particle. Charged particles with and without mass were used in separate simulations. The massless particle is defined as a particle with an invariant mass of zero and carrying an elementary charge of $1.60217646 \times 10^{-19}$ C. For a particle with mass, the actual mass was calculated based on the ratio of charge per unit mass and by assuming an elementary charge of $1.60217646 \times 10^{-19}$ C. The ratio of charge per unit mass for the same poly(vinyl alcohol) used in this work was estimated previously as 96.1 C/kg by Stanger et al. [19], giving a calculated particle mass of 1.67×10^{-21} kg. The starting point of the particle was set at the spinneret which was taken to be the origin (0, 0, 0). The x-y coordinates of the point of "impact" of the particle at the collector (L_{model}) were then plotted as a function of V_d. Comparisons are made between L_{exp} and L_{model} in evaluating the accuracy of the simulations.

RESULTS AND DISCUSSION

A typical electrospinning process produces a round-shaped deposition area with a diameter of about several centimetres. The location of the deposition area on collector corresponds to the closest distance between the spinneret and the collector. When the auxiliary electrodes were charged, it was observed that the deposition area was shifted in the x axis in a direction opposite to the most positive auxiliary electrode. The magnitude of L_{exp} depends on V_d between the auxiliary electrodes. From regression analysis, the magnitude of L_{exp} was found to vary linearly as a function of V_d for both E1 and E2 (*i.e.* ~ 2 mm/kV) (*Figure 3*). A statistically significant linear relationship ($p < 0.05$) between V_d and L_{exp} was observed. Interestingly, the optimal linear fits to the data do not intersect the origin in spite of the symmetrical arrangement used (*Figure 1*). The reason for this is likely to be due to difficulty in repeatability of precisely aligning the experimental setup.

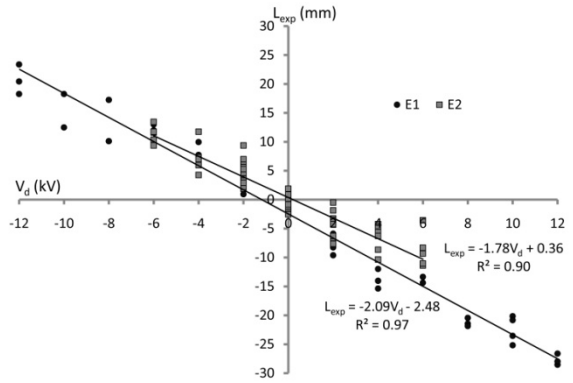

FIGURE 3. The magnitude of shift of the deposition area (L_{exp}) as a function of the voltage difference between the auxiliary electrodes (V_d) for E1 and E2. Solid lines indicate lines of best fit from regression analysis.

It was also observed in E2 that the aspect ratio of the deposition area decreases linearly as V_b increases, changing the shape of the deposition pattern from primarily circular to elliptical. An inverse linear relationship ($p < 0.05$) was observed between the aspect ratio of the deposition area and V_b (*Figure 4*). The observed decrease in the aspect ratio of the deposition area can be described as a "squeezing" effect whereby the lateral electric field constrains the whipping instability region resulting in narrower deposition area.

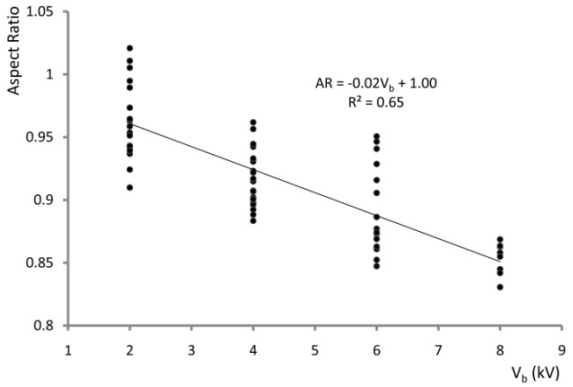

FIGURE 4. The aspect ratio of the deposition area as a function of the base voltage (V_b). Solid line indicates line of best fit from regression analysis.

No statistically significant relationship was found between the aspect ratio and V_d, or between L_{exp} and V_b. The results suggest that V_d and V_b are independent in their action on the electrospun fiber in flight. Hence, V_d and V_b can be considered as two

independent controls *i.e.* V_d as a control of the spatial location of the deposition area whilst V_b as a control of the size of the deposition area.

The application of these controls can produce a wider and uniform deposition area by cyclically varying the applied voltage at the auxiliary electrodes. Furthermore, it is envisaged that the technique can be scaled up by arranging a series of groups of spinnerets within pairs of commonly connected auxiliary electrodes, and by moving the deposition areas to-and-fro in unison to thus eliminate the uneven deposition typically observed in multi-spinneret systems as stripe formation. However it is noted that as the distances between each spinneret to the electrodes varies, the strength of electric field imposed by the electrodes onto each spinneret also varies. It would be expected that at any voltage difference between the electrodes, the outer jets would have a bigger deflection angle compared to the inner jets – this effectively limits the number of spinnerets that can be controlled by a single pair of electrodes. Further studies on quantifying this limit are needed and the results will be reported later.

From SEM images, the typical characteristic of straight PVOH electrospun fibers was shown as a random oriented pattern (*Figure 5*). Results from the SEM Analyser software showed that the measured average of fiber diameter was 340 nm which was within the usual range obtained by the authors' group. The results suggest that the introduction of auxiliary electrodes do not interfere with the natural occurrence of the bending instability which responsible for the thinning and solidifying of the fibers.

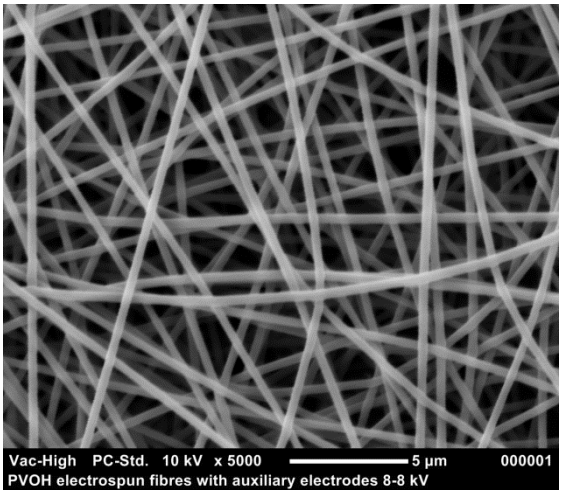

FIGURE 5. The SEM image of electrospun fibers using the apparatus described when both of the auxiliary electrodes were charged at 8 kV.

A simplified FEA model based on the flight of a particle captures the essential changes in flight path with varying electric field distribution. The strength of the electric force exerted on the particle at any point can be determined by using the Lorentz electrical force expression:

$$F = qE \tag{1}$$

and the acceleration imparted by the field to the particle is determined by the equation

$$a = \frac{qE}{m} \tag{2}$$

where, F is the electric force, q is the charge carried by the particle, E is the electric field, a is the acceleration, and m is the mass of the particle.

Due to the alignment of the auxiliary electrodes in the x axis, it was observed experimentally that V_d only influenced L_{exp} in the x axis but not in the y axis. Hence, only E_x is reported in examining the effect of V_d change on the direction of fiber in flight. It has been reported that in both conventional electrospinning [16] and electrospinning through a set of focusing rings [17], the F_z component is the dominant force that draws the fiber toward the collector. However, the F_x component has a significant influence to the deflection direction of the fiber in this study due to varying electric fields imposed by the auxiliary electrodes.

The magnitude of F_x is directly proportional to the x axis component of electric field E_x (Eq. (1)). Therefore, plotting the strength of E_x under different applied voltage conditions at the electrodes would approximately represent the change of electric force experienced by the particle. The magnitude of E_x along the z axis at 10 mm intervals between the spinneret and collector is shown in *Figure 6*. A positive E_x value indicates that the field is acting in the positive x axis direction (or to the left of the experimental setup) and *vice versa* for a negative E_x.

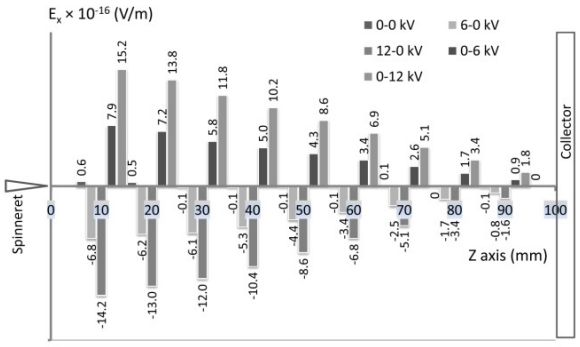

FIGURE 6. The magnitude and direction of x axis electric field components (E_x) along the z axis at 10 mm intervals from the spinneret to collector as a function of V_d.

The magnitude of E_x was negligible along the z axis in the default condition (*i.e.* 0-0 kV), causing no deflection of the particle trajectory (*Figure 6*). Using the voltage combinations as in *Table I*, it was observed in simulations that the magnitude of E_x increased as V_d increased. For example, the magnitude of E_x at a given position along the z axis when V_d=12 kV (*i.e.* 12-0 or 0-12) is approximately double that of V_d= 6 kV (*i.e.* 6-0 or 0-6) (*Figure 6*). The simulation results are coherence with the experimentally observed linear relationships in E1 and E2 where L_{exp} increased when V_d increased (*i.e.* ~ 2 mm/kV).

Due to the auxiliary electrodes' location in relation to spinneret, it is noted that the magnitude of E_x is at a maximum near the spinneret and then reduces to a minimum at the collector (*Figure 6*). This indicates that the influence of manipulated electric field on fiber direction is more significant at early stages of flight than at later stages of flight.

The FEA model is capable of replicating the squeezing effect as evidenced experimentally by a reduction of the aspect ratio of the deposition area. The E_x component of the electric field along x'-x" was significantly increased when V_b increased according to the FEA model (*Figure 7(a)*). A higher E_x peak which correspond to higher electric force (F_x) is produced with a higher applied V_b at the auxiliary electrodes. The force acts to constrain the whipping instability and reduce the size of the deposition area.

The F_y component along y'-y" also increased as V_b increased albeit the magnitude and change in F_y is less than for F_x (*Figure 7(b)*). This examination of E_x and E_y corresponds to the reduction of the deposition area being more significant in the x axis rather than y axis. The reason for this is solely due to the alignment of the auxiliary electrodes in the x axis.

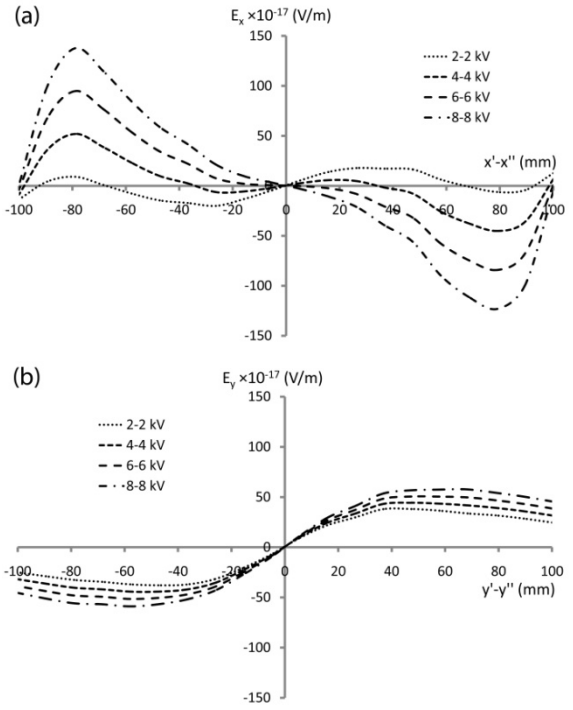

FIGURE 7. The electric field components shown as a function of distance. (a) E_x along x'-x'' and (b) E_y along y'-y''. Note that the resultant E_x and E_y are zero at the centre due to symmetrical alignment of the setup.

A similar deflection response to the applied electric field (*i.e.* the particle moved away from the most positive electrode) was observed in simulations of both E1 and E2 using particles with and without mass. The model depicts the field arrows dispersing evenly from the spinneret towards the collector for the case of a massless particle when both auxiliary electrodes are kept at 0 kV (default condition, E1), causing no deviation in the trajectory of the particle (*Figure 8(a)*). However, the directions of the arrows are deflected to the right from the centre position if a higher voltage is applied to the left electrode (+12 kV) compared to right electrode (0 kV), causing a deviation in the particle trajectory that tends to align with the direction of the electric field (*Figure 8(b)*).

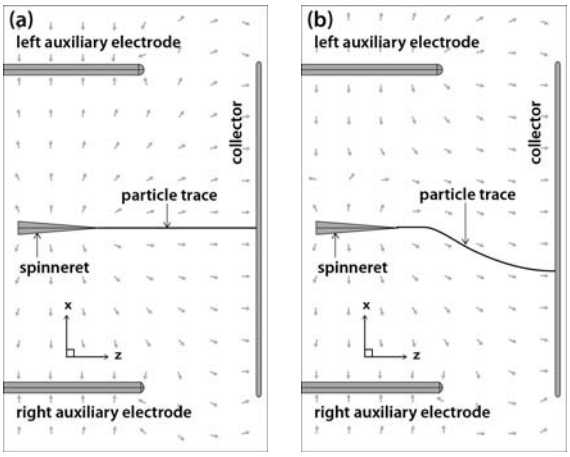

FIGURE 8. The simulated trajectory (solid line) of a charged massless particle (plan view) with voltages of (a) 0-0 and (b) 12-0 kV. The electric field direction is represented by the arrows originating from the higher positive potentials (spinneret or charged electrodes) toward the lower potentials.

Comparisons are made between L_{exp} and L_{model} in evaluating the relationships between experiments and simulations (*Figure 9(a)* and 9*(b)*). As expected, the deflection of the particle without mass was greater than the particle assigned a mass. The gradient of the best fit line for the massless particle was 2.64 compared with 0.41 for the particle with mass for E1 (*Figure 9(a)*). Similarly, the gradient for the massless particle was 2.13 compared with 0.43 for the particle with mass for E2 (*Figure 9(b)*). Clearly, a charged particle with mass has an inertia that decreases its deflection in a given electric field although it does spend more time in the region of transverse electric field compared to a massless particle. A particle without mass will experience infinite acceleration (Eq. (2)) such that the trajectory of the particle simply follows the direction of the electric field lines as observed in the simulations.

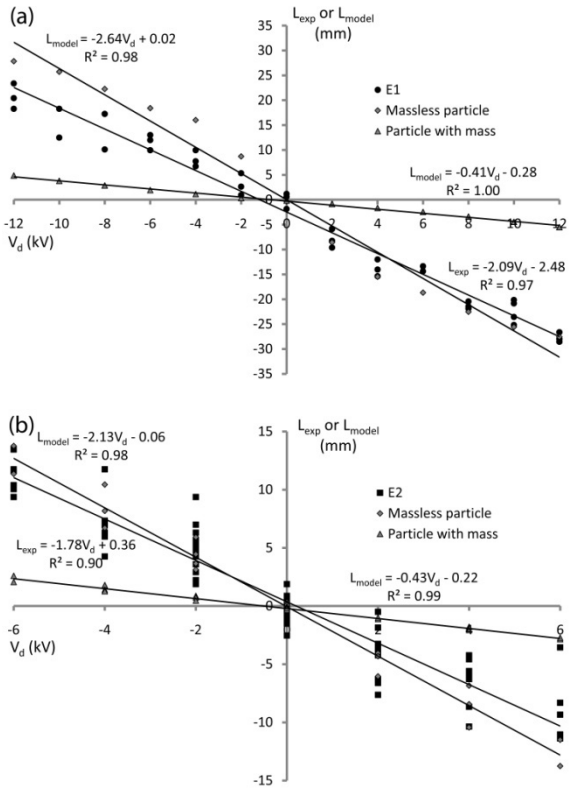

FIGURE 9. L_{exp} and L_{model} as functions of V_d for (a) E1 and (b) E2. Solid lines indicate lines of best fit from regression analysis.

Interestingly, the value of L_{exp} from electrospinning of PVOH correlates more closely with that of a charged particle without mass rather than a charged particle with mass. However, this is thought to be purely coincidental due to the specific experimental set up. Further experiments and simulations were performed using an electrospinning distance of 130 mm to verify this assumption. Additionally, the auxiliary electrodes were shifted 30 mm further away from the spinneret. The spinning voltage was also increased from +10 kV to +12 kV in order to achieve stable electrospinning. The gradients from the linear fits were determined to be 1.53 and 3.15 for the experimental and simulated (massless particle) results, respectively (*Figure 10*). The results confirmed that the correlation found earlier between L_{exp} and a charged particle without mass was coincidental. In the simulation, the extra distance between the spinneret and collector allows more time to the massless particle to travel further before reaching the collector. However, increasing the distances in experiment would only make the control fields less effective to influence the electrospun fiber.

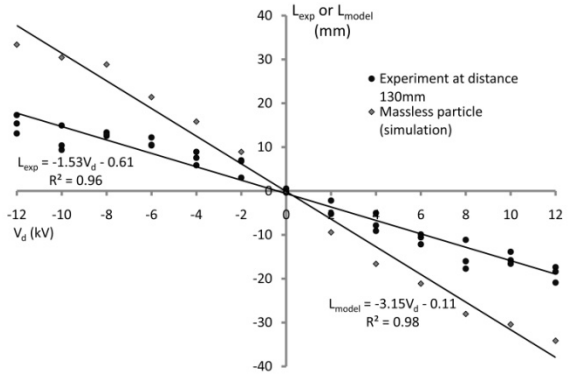

FIGURE 10. L_{exp} and L_{model} as functions of V_d and using a spinneret-collector distance of 130 mm. Solid lines indicate lines of best fit from regression analysis.

It might be expected that a charged particle with mass gives an improved approximation of L_{exp}. However, L_{model} of the charged particle with mass was ~80% less than L_{exp} (*Figure 9(a)* and 9*(b)*). The most obvious reasons are the limitations of the current model used in this study. Although modelling the electrospun fiber as a charged particle provided sufficient insight into the process to produce a practical control algorithm, it is clearly insufficient to replicate the detailed behavior of a continuous charged jet of polymer molecules. If the control algorithm is to be refined, a more complex model is required considering other factors such as solvent loss and the nature of the whipping instability. The magnitude of deflection in an actual electrospinning process is also thought to be magnified by the existence of the whipping instability. In the instability region, the helical-like flight path of the fiber presents itself as a number of individual loops travelling towards the collector. An initial offset between the loops due to lateral electric forces will be magnified by the repulsive forces of like charges, meaning that each loop will also push each other away resulting in a greater deflection of the electrospun fibers. Clearly, a single charged particle-type model does not account for this behavior.

In conducting the simulations, several assumptions have to be made. Within the cubic boundary, the simulation is assumed to take place in free space with no atmosphere or gas of any kind so deflection of the particle trajectory which may be caused by friction with air molecules can be neglected. No loss of electric charge to the surroundings occurs and the effect of other geometries in the experimental setup is not considered to be significant.

Linear regression adequately describes the relationship between L_{model} in response to V_d. However, the fitting of polynomial curves appears to improve the fit slightly. A charged particle has a trajectory through space that depends on the applied electric field. As the V_d varies, a higher applied voltage could lead to the charged particle spending less time in the region of higher electric field strength. This is the probable reason for the relationship being slightly non-linear. Nevertheless, the difference between values from the linear and polynomial models is smaller than the maximum standard deviation of the experimental data. Moreover, fitting of linear models to the data produces adjusted R^2 values close to unity (0.98-1.00).

CONCLUSION

Experimental and simulation studies of the control of the spatial location and size of the deposition area *via* electric field manipulation were the focus of this work. The main conclusions from this study are as follows:

- It was observed experimentally that the location of the deposition area moved linearly ($p<0.05$) with voltage difference V_d between the auxiliary electrodes, and the aspect ratio of the deposition area reduced linearly ($p<0.05$) with base voltage V_b;
- From the FEA results, it is shown that the x-axis component of electric field (E_x) which correspond to electric force F_x was responsible for the change in location and the reduction of aspect ratio of the deposition area;
- Although a simplified particle-model was unable to predict the precise location of the fiber deposition position, FEA was useful for broadly describe the movement of electrospun fibers in flight in response to varying electric fields; and
- The application of the technique described in this study can potentially be used in large scale production for producing uniform electrospun fiber membranes. The authors note that significant work has previously been done to produce uniform distribution of fibers from multi-spinnerets on the industrial scale and that the scale up of our process will be a distinctly a non-trivial task. Further studies on the matter are ongoing and the results will be reported elsewhere.

ACKNOWLEDGEMENT
The authors acknowledge the financial support of the Ministry of Higher Education of Malaysia, the Dick and Mary Earle Scholarship and The New Zealand Ministry of Science & Innovation (Contract C11X1001—Electrospun fibers for surface-active materials). The authors also thank Electrospinz Ltd. (Blenheim) for equipment support, Alasdair Noble for his assistance with statistical analysis and Donna Gibson for graphic illustrations.

REFERENCES
[1] Doshi, J., Reneker, D. H., Electrospinning Process and Applications of Electrospun Fibers. *J Electrostat* 1995, *35*, 151-160.
[2] Tucker, N., Stanger, J. J., Staiger, M. P., Razzaq, H., Hofman, K., The History of the Science and Technology of Electrospinning from 1600 to 1995. *Journal of Engineered Fibers and Fabrics, Special Fibers Edition* 2012, *7*, 63-73.
[3] Cooley, J. F., *UK Patent GB06385*, United Kingdom 1900.
[4] Morton, W. J., *US patent US705691*, United States 1902.
[5] Formhals, A., *US Patent US1975504*, United States 1934.
[6] Taylor, G., Disintegration of Water Drops in an Electric Field. *Proceedings of the Royal Society of London A: Mathematical, Physical & Engineering Sciences* 1964, *280*, 383-397.
[7] Ramakrishna, S., Fujihara, K., Teo, W. E., Lim, T. C., Ma, Z., *An introduction to electrospinning and nanofibers*, World Scientific, Hackensack, NJ ; London 2005.
[8] Theron, S. A., Yarin, A. L., Zussman, E., Kroll, E., Multiple Jets in Electrospinning: Experiment and Modeling. *Polymer* 2005, *46*, 2889-2899.
[9] Filatov, Y., Budyka, A., Kirichenko, V., *Electrospinning of Micro and Nanofibers: Fundamentals and Applications in Separation and Filtration Processes*, Begell House Inc., New York 2007.
[10] Petrík, S., in: Lin, T. (Ed.), *Nanofibers - Production, Properties and Functional Applications*, InTech 2011, pp. 1-16.
[11] Niu, H. T., Lin, T., Fiber Generators in Needleless Electrospinning. *J Nanomater* 2012.
[12] Deitzel, J. M., Kleinmeyer, J. D., Hirvonen, J. K., Tan, N. C. B., Controlled Deposition of Electrospun Poly(ethylene oxide) Fibers. *Polymer* 2001, *42*, 8163-8170.
[13] Bellan, L. M., Craighead, H. G., Control of an electrospinning jet using electric focusing and jet-steering fields. *J Vac Sci Technol B* 2006, *24*, 3179-3183.
[14] Kim, G., Cho, Y. S., Kim, W. D., Stability Analysis for Multi-jets Electrospinning Process Modified with a Cylindrical Electrode. *Eur Polym J* 2006, *42*, 2031-2038.
[15] Nurfaizey, A. H., Stanger, J., Tucker, N., Buunk, N., *et al.*, Manipulation of electrospun fibers in flight: the principle of superposition of electric fields as a control method. *Journal of Materials Science* 2012, *47*, 1156-1163.
[16] Heikkila, P., Soderlund, L., Uusimaki, J., Kettunen, L., Harlin, A., Exploitation of electric field in controlling of nanofiber spinning process. *Polym Eng Sci* 2007, *47*, 2065-2074.
[17] Cui, X. J., Li, L. M., Xu, F., Controlled assembly of poly(vinyl pyrrolidone) fibers through an electric-field-assisted electrospinning method. *Appl Phys a-Mater* 2011, *103*, 167-172.
[18] Angammana, C. J., Jayaram, S. H., The Effects of Electric Field on the Multijet Electrospinning Process and Fiber Morphology. *Ieee T Ind Appl* 2011, *47*, 1028-1035.
[19] Stanger, J., Tucker, N., Fullick, S., Sellier, M., Staiger, M. P., Insights into the power law relationships that describe mass deposition rates during electrospinning. *J. Mater. Sci.* 2012, 1113-1118.

AUTHORS' ADDRESSES
Abdul Hamid Nurfaizey
Jonathan Stanger
Mark P. Staiger
Department of Mechanical Engineering
University of Canterbury
Christchurch 8020
NEW ZEALAND

Abdul Hamid Nurfaizey
Faculty of Mechanical Engineering
Universiti Teknikal Malaysia Melaka
76100 Melaka
MALAYSIA

Abdul Hamid Nurfaizey
Jonathan Stanger
Nick Tucker
The New Zealand Institute for Plant & Food Research Limited
Gerald Street
Lincoln 7608
NEW ZEALAND

Jonathan Stanger
Neil Buunk
Electrospinz Ltd
Blenheim
NEW ZEALAND

Alan R. Wood
Department of Electrical and Computer Engineering
University of Canterbury
Christchurch 8020
NEW ZEALAND